Analyst

Accepted Manuscript

This article can be cited before page numbers have been issued, to do this please use: B. R. Adhikari, H. Schraft and A. Chen, *Analyst*, 2017, DOI: 10.1039/C7AN00594F.

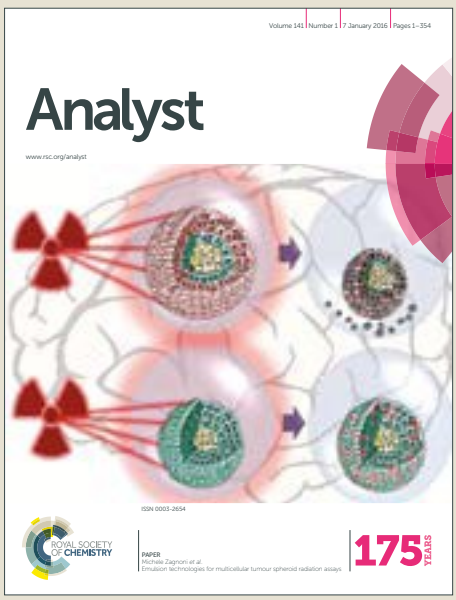

ROYAL SOCIETY OF CHEMISTRY

rsc.li/analyst

View Article Online
DOI: 10.1039/C7AN00594F

Journal Name

ARTICLE

High-performance enzyme entrapment platform facilitated by a cationic polymer for the efficient electrochemical sensing of ethanol

Received 00th January 20xx,
Accepted 00th January 20xx

DOI: 10.1039/x0xx00000x

www.rsc.org/

Bal-Ram Adhikari,[a] Heidi Schraft,[b] Aicheng Chen*[a]

Entrapment is one of the major approaches for enzyme immobilization; however, it suffers a few critical drawbacks including leakage and high mass transfer resistance to substrate. To address those challenges, herein we report on a new facile and effective enzyme entrapment platform using a special cationic polymer, poly(2-(dimethylamino) ethyl methacrylate) (MADQUAT) on a single-wall carbon nanotube and reduced graphene oxide (SWCNT-rGO) nanohybrid thin film. To demonstrate this new approach, alcohol dehydrogenase (ADH) is employed as a model enzyme for the entrapment toward the design of an efficient electrochemical biosensor for the detection of ethanol. MADQUAT possesses strong electrostatic affinity with various negatively charged biomolecules; and our FTIR study has shown that there are no structural changes in enzyme following the entrapment, with an excellent secondary structure association (r = 0.92). Our electrochemical measurements have shown that the entrapped ADH exhibits high ability to exchange electrons in presence of the NAD^+/NADH cofactor and that the SWCNT-rGO nanohybrid significantly enhances the biocatalytic activity of the immobilized ADH and the electrochemical oxidation of NADH in comparison with either SWCNTs or rGO. The ethanol biosensor developed in this study exhibits a fast response, wide linearity range, high sensitivity (26.27 μA mM^{-1} cm^{-2}), remarkable low limit of detection (0.16 μM), high selectivity and high stability. The optimized biosensor has been further tested with real samples including wine, beer and blood alcohol, showing promising analytical and biomedical applications.

Introduction

Cationic polymers such as poly(amidoamine) (PAMAM), protamine sulfate, poly(L-lysine) (PLL), chitosan derivates, poly(ethylenimine) (PEI), and MADQUAT have been explored as non-viral carriers for gene delivery.[1] These cationic polymers have strong electrostatic interaction with different negatively charged molecules, particularly in blood components like red blood cells (RBCs) or plasma proteins.[2] There is a great interest in developing high-performance electrochemical biosensors for medical and environmental applications. Entrapment is one of facile methods for enzyme immobilization; however, enzyme leakage and sluggish substrate-enzyme active site mass transfer are the two major issues with the existing entrapment based electrochemical biosensors.[3,4] Although MADQUAT is a cationic polymer and has strong electrostatic affinity with various negatively charged biomolecules, to the best of our knowledge, there is no report on its utilization in entrapment of enzyme for biosensor fabrication.

Blood alcohol determination plays an important role in forensic and laboratory medicine; drunk driving is a serious problem in the modern world, which results in many fatal accidents each year. In addition, it is necessary in clinical laboratories for the detection of acute alcoholism and syndromes that are related to alcohol abuse. Presently, many methods have been employed for the quantification of alcohol levels, including spectrometric, chromatographic and colorimetric analysis. However, these methods are time consuming and complex to perform due to laborious sample pre-treatment and expensive analytical instrumentation. Thus, there is an increasing requirement for rapid, accurate, and inexpensive methods for the determination of alcohol.[5] Electrochemical biosensors are attractive alternatives for biomolecules monitoring as they may provide specific, rapid, and repetitive assays through the use of low-cost miniaturized transducers.[6,7]

Ethanol biosensors are typically based on NAD-dependent alcohol dehydrogenase.[8-11] NAD-dependent oxidoreductases exist in

[a] Department of Chemistry, Lakehead University, 955 Oliver Road, Thunder Bay, OntarioP7B 5E1, Canada. E-mail: aicheng.chen@lakeheadu.ca (A. Chen).Tel.:+1 807 3438318; Fax: +1 807 3467775.
[b] Department of Biology, Lakehead University, 955 Oliver Road, Thunder Bay, OntarioP7B 5E1, Canada.

† Electronic supplementary information (ESI) available: Secondary structure composition of alcohol dehydrogenase (ADH) as calculated by fitting the amide I region (Table S1); Comparison of the performance of various electrodes for the electrochemical sensing of ethanol (Table S2); CV responses of a bare GC electrode, and GC electrodes modified with rGO, SWCNTs and SWCNT-rGO nanohybrid recorded in a 0.1 M KCl solution containing 2.5 mM $K_3Fe(CN)_6$ at the scan rate of 20 mV s^{-1} (Fig. S1); CVs of the ADH-SWCNT-rGO/GCE recorded in 0.1 M tris buffer (pH 8.2) containing 50 mM ethanol and 10 mM NAD^+ at different scan rates of 20, 30, 40, 50, 60 and 70 mV s^{-1} (Fig. S2)

View Article Online
DOI: 10.1039/C7AN00594F

virtually all organisms and catalyze the reversible oxidation of primary and secondary alcohols into aldehydes and ketones, respectively. Medium-chain alcohol dehydrogenases (ADHs, EC 1.1.1.1) contain 327−376 amino acid residues per chain and are generally zinc-dependent.[9] Yeast alcohol dehydrogenase (ADH1) is a tetramer of four identical subunits that contain 347 amino acid residues each, with an estimated mass of 147396 Da.[12,13] Electrochemical enzyme-based biosensors combine the high specificity of enzymes with the sensitivity of electrochemical transducers. Enzyme electrodes are electrochemical probes that incorporate a thin layer of immobilized enzymes on the surface of the working electrode.[14] Alcohol dehydrogenase (ADH) based biosensors have been extensively employed for the determination of ethanol for many years due to their cost effectiveness, rapidity, reliability, and specificity. In these types of biosensors, ADH catalyzes the oxidation of ethanol to acetaldehyde in the presence of NAD^+. The generated NADH in the reaction can be detected amperometrically following the application of a suitable potential to the electrode.[15-18]

Nanocomposites/hybrids can often combine the advantages of their constituent components to exhibit enhanced properties.[19-21] SWCNTs, which consist of single graphene sheets that are seamlessly wrapped into cylindrical tubes with diameters of between 0.4 and 2.5 nm, offer excellent physical and chemical properties that enable a wide range of biomedical applications.[22,23] Graphene nanosheets are one-atom thick planar sheets of sp^2-bonded carbon atoms that are attracting tremendous attention in terms of fundamental research and potential applications.[24-26] The high surface to volume ratio of nanomaterials along with layered structure contributed to the highly sensitive chemical/biospecies interaction; atomically thick graphene sheets provide extremely high surface areas and abundant surface-resident atoms for electron transport, which make them highly sensitive to detect target molecules.[27-29] CNTs and GO share many similar properties, while being structurally dissimilar, rGO/CNT non-covalent composites provides significantly higher heterogeneous electron transfer (HET) rate with great potential to be utilized in high-performance biosensor fabrication.[30]

In the present study, we have proposed a new enzyme entrapment platform based on the SWCNT–rGO nanohybrid with the assistance of the MADQUAT polymer. The entrapped ADH was assessed for any conformational changes through secondary structure analysis, revealing no structural changes. A significant synergistic enhancement of the SWCNT-rGO nanohybrid was confirmed, and the ADH entrapped by MADQUAT showed high sensitivity, selectivity and stability for the detection of ethanol.

Experimental Section

Chemicals and reagents

Graphite powder, SWCNTs (Ø0.7 nm), Poly(2-(dimethylamino)ethyl methacrylate (MADQUAT), ADH from *Saccharomyces cerevisiae (EC 1.1.1.1),* β-nicotinamide adenine dinucleotide hydrate (NAD^+), human serum (from human male AB Plasma), ethanol (98%) and Trizma base were purchased from Sigma-Aldrich. All chemicals used were of analytical grade, and all solutions and buffers were prepared with double deionized (DI) water (Nanopure® water purification systems).

Apparatus

All electrochemical experiments, including cyclic voltammetry (CV) and amperommetry were performed using a CHI 660 electrochemical workstation (CH Instruments Inc., USA) using a conventional three-electrode system that consisted of a platinum wire counter electrode, a 3.0 M KCl saturated Ag/AgCl reference electrode, and a working electrode comprised of a modified Ø3 mm glassy carbon electrode (GCE). X-ray diffraction (XRD) was used to characterize the synthesized graphene oxide (GO). Fourier transform infrared spectroscopy (FTIR, Nicolet) equipped with a liquid N_2-cooled MCT detector was employed for the study of the enzyme-MADQUAT interaction. The estimation of the secondary structure composition was carried out by the curve fitting of the amide I bands using the peak fitting software (SeaSlove Software Inc., USA), where the deconvoluted parameters were set with a gamma value of 1.65 with a smoothing length of 55 and the second derivative spectra were calculated over a 13-data-point range (13 cm^{-1}).[31] A field-emission scanning electron microscope (FE-SEM) (Hitachi SU-70) was employed for the surface characterization of the SWCNT-rGO nanohybrid. All experiments were performed at room temperature and all of the potentials quoted are versus the Ag/AgCl reference electrode.

Fabrication of biosensor

The graphite oxide was synthesized using the simplified Hummer's method [32] and the GO suspension was prepared by ultrasonicating 5.0 mg of the graphite oxide powder in 1.0 ml DI water for 30 min. The SWCNT suspension was prepared by ultrasonicating 5.0 mg mL^{-1} of SWCNTs in dimethylformamide (DMF) for 30 min. Tris buffer solutions (0.1 M) for the electrochemical studies was prepared using a Trizma base and adjusted the pH to 8.2 using 1 M HCl. The carbon nanohybrids were formed on GCE by drop-casting and drying 1:1 v/v ratio of the GO and SWCNT suspension (2.0 µL each), and then reduced by running CV in the potential range of -0.6 to -1.5 V for five cycles at 20 mV s^{-1} in 0.1M tris buffer solution after purging with Argon gas for 10 min. For comparison, the GC electrodes modified with individual rGO and SWCNT were prepared using the same approach, while 4.0 µL of the GO and SWCNT suspensions was cast. The ADH was immobilized by incubating 2.0 µL ADH (5.0 mg mL^{-1}) with 2.0 µL MADQUAT (50 mg ml^{-1}) over the GCE surface that was modified with the rGO, SWCNT, and SWCNT-rGO thin films. Incubation was performed in a 4 ^oC refrigerator for 30 min, followed by rinsing with the tris buffer.

Result and Discussion

Characterization of SWCNT-rGO nanohybrid on the GCE surface

The morphologies of the individual rGO and SWCNT films and the SWCNT–rGO nanohybrid were characterized via FE-SEM. Fig. 1A displays the SEM image of the rGO formed on the GCE surface,

View Article Online
DOI: 10.1039/C7AN00594F

revealing a rippled-like surface structure, which is a typical feature of pristine graphene. Fig. 1B depicts a FE-SEM image of SWCNTs,

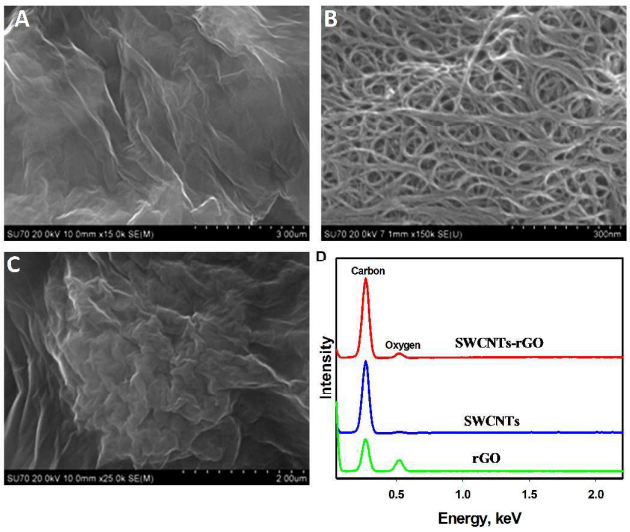

Fig. 1. SEM images of (A) rGO, (B) SWCNTs and (C) SWCNT-rGO nanohybrids; (D) EDX spectra of rGO (green), SWCNTs (blue) and SWCNT-rGO nanobybrid (red).

showing the GCE surface was homogeneously covered by the carbon nanotubes. Fig. 1C shows the nanohybrid film, in which rGO sheets were uniformly dispersed throughout the SWCNTs. The typical aggregation and distinctive formation between individual rGO layers were inhibited in the SWCNT–rGO nanohybrid film due to the presence of the SWCNTs, leading to the enhancement of the specific surface areas and porosity**.** Fig. 1D presents the energy dispersive X-ray (EDX) spectra of the SWCNT-rGO nanohybrid (red), as well as isolated SWCNTs (blue), and rGO (green).Their oxygen : carbon ratio was decreased in the following order: rGO > SWCNT-rGO > SWCNTs, Indicating the oxygen functional groups of the GO was partially removed during the electrochemical reduction treatment.[33]

In order to investigate the electrochemical behaviors of the SWCNT-rGO nanohybrid thin film, CV (Supplementary Fig. S1) was performed with the $[Fe(CN)_6]^{3-}/^{4-}$ couple as the redox probe. The CVs of the GC electrode (blue), as well as those modified with SWCNT-rGO nanohybrid (pink), SWCNTs (sky blue), and rGO (red), were recorded in 2.5 mM $K_3Fe(CN)_6$ + 0.1 M KCl. The peak potential separation (ΔE_p) between the anodic (Epa) and cathodic (Epc) peak among the nanohybrid, SWCNTs and rGO remained ~55 mV but with significantly increased current response at the SWCNT-rGO nanohybrid as compared to the GCE that was modified with SWCNTs or rGO nanosheets alone. In contrast, a low current response with a large peak separation was observed at the bare GCE. The significant increase of the current response and the decrease of the peak separation show that the SWCNT-rGO nanohybrid provide a desirable platform with high conductivity and a large surface area for enzyme immobilization

Structural studies of the immobilized ADH

The immobilization method is an important factor, which determines the electron transfer rates between electrodes and

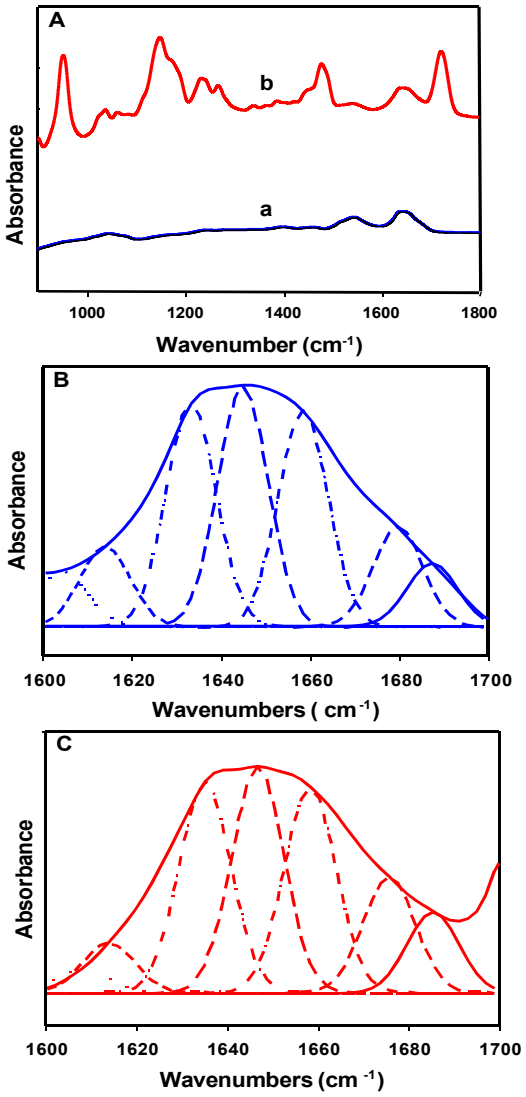

Fig. 2. (A) FTIR spectra of ADH: free (a), and after being entrapped on the SWCNT-rGO nanobybrid film by MADQUAT (b). Deconvoluted FTIR spectra in the amide I region together with the respective best-fitted individual band components of the free (B) and entrapped (C) ADH

the enzymes.[34] Among various immobilization techniques, the entrapment of enzymes within the polymer matrix yielded higher electron transfer compared to physisorbed enzymes.[35] The polymer backbone supporting the methacrylate in MADQUAT were attached with non-covalent polar π interactions.[36] The nanohybrid structure provides a unique π-π hydrophobic interaction to communicate with polymer and enzyme. MADQUAT is a cationic polymer, composed of cationic functional groups. These cationic functional groups interact with negatively charged amino acid chains of ADH in tris buffer, whose pH was higher than the isoelectric point of ADH (pI 5.4-5.8). The strong electrostatic self-

View Article Online
DOI: 10.1039/C7AN00594F

assembly of MADQUAT with ADH makes it possible to design an advanced platform for ethanol detection. The conformational changes of the enzymes upon immobilization were investigated, in comparison to their native structures in aqueous media. Fig.2A shows the FTIR spectra of the pure ADH enzyme in aqueous media (a) (pH 8.2, tris buffer 0.1M) and the immobilized ADH (b). The analysis of the amide I band in the range of 1600–1700 cm^{-1} (due to the C=O stretching vibration) makes it possible to study the effect of immobilization on the secondary structure of the protein.[37] The amide I band consisted of several overlapping components that were assigned to different secondary structural elements. These individual components were identified from the second-derivative spectra. The bands at 1610–1640 cm^{-1} and 1685–1695 cm^{-1} were assigned to β-sheets, at 1640–1650 cm^{-1} to random coils, at 1650–1660 cm^{-1} to α-helix, and at 1660–1685 cm^{-1} to β–turns.[38] In order to estimate the secondary structural composition of the enzyme, a curve fitting of the deconvoluted amide I region was performed through the software aforementioned in experimental section for ADH in the aqueous solution (Fig. 2B) and the immobilized ADH (Fig. 2C). The secondary structural information following the deconvolution of the amide I region obtained from Figs. 2B and 2C are presented in supplementary Table S1. As shown in Table S1, the free ADH in the aqueous solution had a high β-sheet (29%) content, in comparison to α-helix (22%), followed by 25% randomly coiled structures, and 11% β-turns. The components derived from α-helix structures were an excellent indicator of the desirable folding of the enzyme; the loss of this secondary structure typically leads to enzyme inactivation. As seen in Table S1, α-helix content present in the aqueous ADH (22%) and the immobilized ADH (21%) was almost identical, revealing the desirable folding of the enzyme after being entrapped on the SWCNT-rGO nanohybrid film with the assistance of the new polymer MADQUAT. Only a minor decrease of β-sheet from 25% to 23% and a small increase of β-turn content from 11% to 14% were observed following the immobilization. The slight variances in secondary structural changes observed were likely related to transesterification activity expressed by the enzyme subsequent to its immobilization.[39] To verify the positive association between both secondary structural panels, we further calculated the correlation coefficient (r) value; and the high r value (0.92) indicated that the structure of the immobilized enzyme was not significantly altered.

Electrocatalytic behaviour of ADH onto SWCNT-rGO nanohybrid for ethanol detection

Fig. 3 presents the CVs of the GCE modified with MADQUAT entrapped ADH onto rGO (A), SWCNTs (B), SWCNT-rGO nanohybrid (C) recorded in 10 mM NAD^++ 0.1 M trish buffer in the presence of 50 mM ethanol (red solid line) and in the absence of ethanol (blue dashed line) at a scan rate of 20 mVs^{-1}. The ADH immobilized on the SWCNT-rGO nanohybrid showed a distinct and much stronger NADH oxidation peak at ~0.41V in the presence of ethanol (Fig. 3C), in comparison to the ADH entrapped on SWCNTs (Fig. 3B), whereas almost no oxidation peak was observed for the ADH entrapped on the rGO (Fig. 3A).

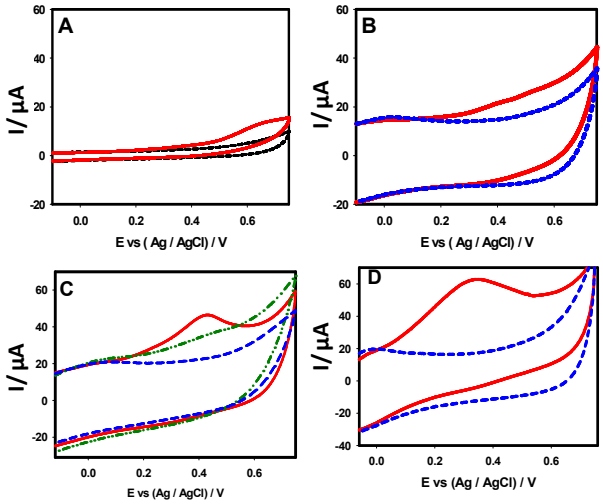

Fig.3. Cyclic voltammograms of the GC electrodes modified with (A) ADH-rGO, (B) ADH-SWCNT and (C) ADH-SWCNT-rGO nanohybrid (entrapped ADH-red solid line); physisorbed ADH (green dashed line) in a 0.1M tris buffer containing 50 mM ethanol + 10 mM NAD+ and only 10 mM NAD+(blue dashed line). (D) CV of the SWCNT-rGO without ADH recorded in a 0.1M tris buffer in the absence of NADH (blue dashed line) and in the presence of 10 mM NADH (red solid line). The scan rate was 20 mV s^{-1}.

The performance of physisorbed ADH on the SWCNT-rGO nanohybrid (green dashed line) has also been compared with the MADQUAT entrapped ADH on the SWCNT-rGO nanohybrid (red solid line) in Fig. 3C, revealing that the MADQUAT entrapped ADH on the SWCNT-rGO nanohybrid exhibited a significant improvement in performance over the physisorbed ADH. Fig. 3D displays the direct NADH oxidation on the MADQUAT-SWCNT-rGO nanohybrid thin film without the enzyme in presence of 10.0 mM NADH in 0.1M tris buffer (pH 8.2), further confirming that the large well-defined peak appeared in Fig. 3C was due to the oxidation of NADH generated by the immobilized ADH during the ethanol oxidation. The mechanisms of ethanol oxidation catalyzed by ADH, which contains four different subunits that are arranged as two dimers albeit structurally similar (Scheme 1). Each subunit within the dimers encompasses a coenzyme (NAD^+) binding domain, which is typical of the Rossmann fold (six-stranded parallel β-pleated sheets with two helices on both sides of the sheets) to which the coenzyme is bound at the terminal ends of the carboxyl. Each subunit also possesses a catalytic domain that contains zinc to which alcohol binds, and the substrates bind within the clefts between the domains.[40] Ethanol oxidation proceeds through the deprotonation of nicotinamide ribose by His-51, Ser-48 by nicotinamide ribose, and alcohol by Ser-48, in sequential order.[41]

The hydride transferring from the alkoxide ion to NAD^+ leads to the formation of NADH and aldehyde or ketone being bound to NAD^+

View Article Online
DOI: 10.1039/C7AN00594F

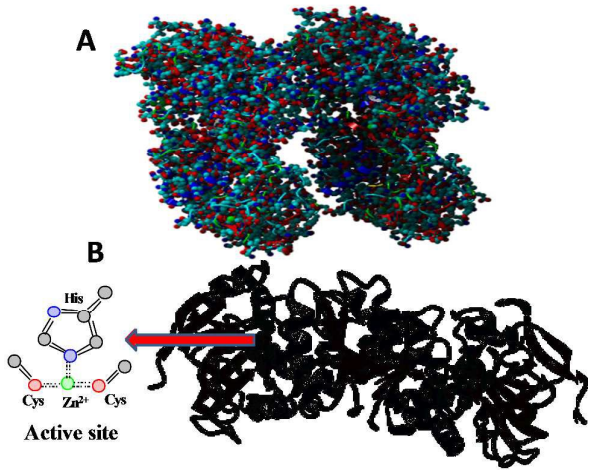

Scheme 1. (A) Tetramer structure of ADH; and (B) Active sites of the ADH enzyme.

leads to the formation of NADH and aldehyde or ketone being bound to the zinc active site. ADH typically catalyzes ethanol oxidation via the following bi-bi mechanism:[42]

$$E + A + B \rightleftharpoons EA + B \rightleftharpoons EAB \rightleftharpoons EPQ \rightleftharpoons EQ + P \rightleftharpoons E + P + Q$$

where E is the enzyme; A represents β-NAD^+; B denotes the alcohol; whereas P and Q are the products of acetaldehyde and NADH. In our case, the overall reactions at the electrode/electrolyte interface may be described as follows:

$$CH_3CH_2OH + NAD^+ \xrightarrow{ADH} CH_3CHO + NADH + H^+$$

$$NADH \longrightarrow NAD^+ + H^+ + 2e^-$$

The ADH immobilized on the SWCNT-rGO nanohybrid film effectively catalyzed the oxidation of ethanol to acetaldehyde and the conversion of NAD^+ to NADH. The NAD^+ was regenerated via the electrochemical oxidation of the formed NADH, where a two-electron transfer was involved.

To understand the effect of the amount of MADQUAT used for the entrapment of ADH on the SWCNT-rGO nanohybrid, five different concentrations (5.0, 20.0, 30.0, 50.0, and 60.0 mg mL^{-1}) of MADQUAT were used, while the ADH concentration was kept constant (5.0 mg mL^{-1}). Fig.4A presents the amperometric responses of the modified electrodes measured in a 20 µM ethanol + 10 mM NAD^+ solution. The peak current was increased with the increase of the concentration of MADQUAT from 5.0 to 50.0 mg mL^{-1}, which may be attributed to the increase of the electrostatic force of the polymeric cations and the enzymatic anions, thus lowering the zeta potential between ADH and MADQUAT. However, the current response was slightly decreased when the MADQUAT concentration was increased from 50.0 to 60.0 mg mL^{-1}, which might result in imbalance of the cationic/anionic ratio between polymer and enzyme, thus lowering their electrostatic force and increasing the zeta potential.[43]

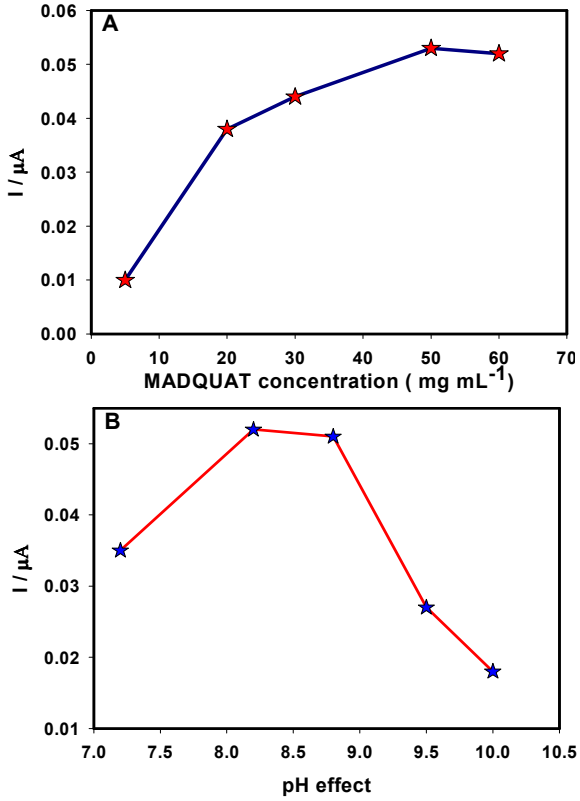

Fig. 4. (A) Effect of the concentration of MADQUAT used for entrapping ADH on the SWCNT-rGO/GCE on the peak current measured in a 0.1M tris buffer containing 20 µM ethanol and 10 mM NAD^+. (B) Effect of pH (7.2, 8.2, 8.8, 9.5 and 10) on ADH-SWCNT-rGO/GCE in a 0.1M tris buffer containing 20 µM ethanol and 10 mM NAD^+; E_{app} 0.5 V.

Hence, 50.0 mg mL^{-1} MADQUAT was chosen as the optimum concentration for the entrapment of the enzyme ADH. The effect of pH on the biosensor was investigated in 20 µM ethanol + 10 mM NAD^+ solution. As shown in Fig. 4B, the response was increased with the increase of the pH from 7.2 to 8.2; but it was decreased with the further increase of the pH from 8.8 to 10.0., indicating that 8.2 was the optimized pH.

The effect of the scan rate on the electrochemical behavior of the MADQUAT entrapped ADH on the SWCNT-rGO nanohybrid was investigated in a 0.1 M tris buffer (pH 8.2) containing 50mM ethanol and 10mM NAD^+. As shown in Fig. S2A, the peak current due to the anodic oxidation of NADH was in elevated with the increase of the scan rate from 20 to 70 mVs^{-1}, whereas the peak potential gradually shifted toward more positive. The plot of anodic peak current versus the scan rate (Supplementary Fig. S2B) exhibited a linear relationship (R^2 = 0.997), showing that the electrochemical oxidation was a surface-controlled process.

Performance of the ethanol biosensor

The analytical performance of the prepared ethanol biosensor was assessed using CV and amperometry. Fig.5A displays the CV

View Article Online
DOI: 10.1039/C7AN00594F
Journal Name

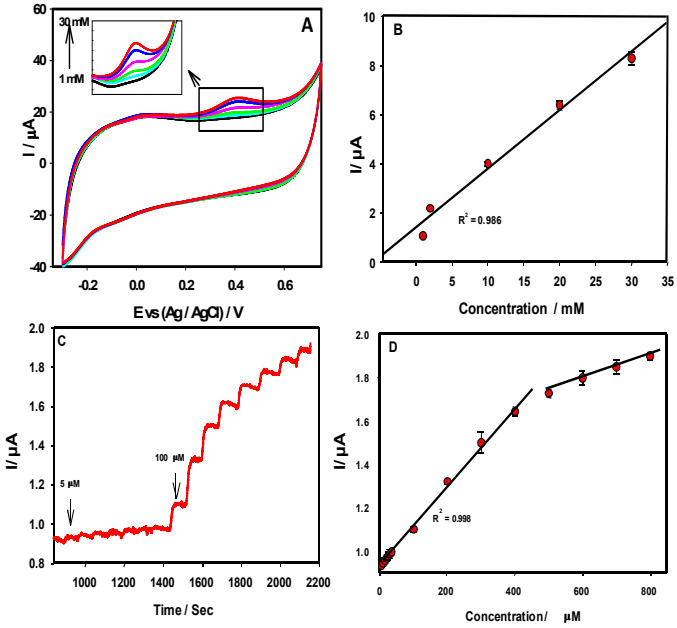

Fig. 5. (A) CV responses at the scan rate of 20 mV s^{-1} of the ADH-SWCNT-rGO/GCE in 0.1M tris buffer (pH 8.2) containing different concentrations of ethanol (1 – 30 mM) + 10 mM NAD^+. (B) Calibration plot of the current responses derived from Fig. 5A. (C) Amperometric responses of the optimized ADH-SWCNT-rGO/GCE to the successive addition of ethanol varied from 5 - 800 µM into a 0.1M tris buffer (pH 8.2) + 10 mM NAD^+(E_{app}= 0.5V). (D) Calibration plot of the current responses derived from Fig. 5C.

responses to the successive addition of ethanol (1mM to 30 mM) into a 0.1M tris buffer (pH 8.2) containing 10 mM NAD^+. The analytical performance of the prepared ethanol biosensor was assessed using CV and amperometry. Fig.5A displays the CV responses to the successive addition of ethanol (1mM to 30 mM) into a 0.1M tris buffer (pH 8.2) containing 10 mM NAD^+. For clarification, the oxidation peak range of the CV was enlarged and is presented as an inset of Fig. 5A, showing that the current was increased with the increase of the ethanol concentration. A linear increment of the current response with R^2= 0.986 was attained with the sensitivity of 0.26 µA mM^{-1}as seen in Fig. 5B. The limit of detection (LOD) was estimated to be 110 µM based on a signal-to-noise ratio of 3σ/b, where σ is standard deviation of blank and b is slope value obtained through calibration curve. The wide detection range obtained through CV might be utilized for the serum level detection of ethanol, especially for road safety and medical purposes. According to the International Center for Alcohol Policies (ICAP), an average serum level of >17.4 mM is considered as unsafe for driving in Canada and USA. Amperometric technique was employed to detect the comparatively low concentration range of ethanol. To optimize the applied electrode potential, four different electrode potentials including 0.40, 0.45, 0.50 and 0.55 V were evaluated for the amperometric detection of 50 µM ethanol in 0.1M tris buffer (pH 8.2) containing 10mM NAD^+. The amperometric current response was increased with the increase of the potential from 0.40 to 0.50V; however, the current response remained almost constant when the potential was further increased from 0.50 to 0.55 V. Therefore, 0.5V was chosen as the optimum potential for all the amperometric measurements as displayed in Fig. 5C, where rapid response was observed after the addition of ethanol. The corresponding calibration plot is presented in Fig. 5D, showing two linear regression ranges. The LOD value of 0.16µM with a sensitivity of 1.84 µA mM^{-1} was achieved in the concentration from 5 - 400 µM with R^2= 0.998.

The LOD, sensitivity and linear detection range obtained with this study was superior to those reported in the literature,[15,44-49] as listed in supplementary Table S2. The amperometric response of ethanol at the concentration 400 µM gave a characteristic plateau current, showing the pattern of Michaelis–Menten kinetics as seen in Fig. 5D. The Michaelis-Menten constant (K_m) of the enzymatic reaction was calculated using the Lineweaver–Burk equation:[50]

$$\frac{1}{I_{ss}} = \frac{K_m}{I_{max}} \times \frac{1}{C} + \frac{1}{I_{max}}$$

where K_m is the Michaelis-Menten constant, I_{ss} is the steady state current, I_{max} is the maximum current obtained and c is the concentration of the substrate (ethanol). The K_m value calculated in this study for immobilized ADH on SWCNT-rGO nanohybrid was 0.088 mM. This value was much lower than those typically reported in the literature.[34,48,51] All of the parameters obtained through different techniques indicated that the ADH-SWCNT-rGO biosensor exhibited a high enzymatic activity toward the ethanol detection over a wide range of concentrations, which makes it useful for various ethanol sensing applications.

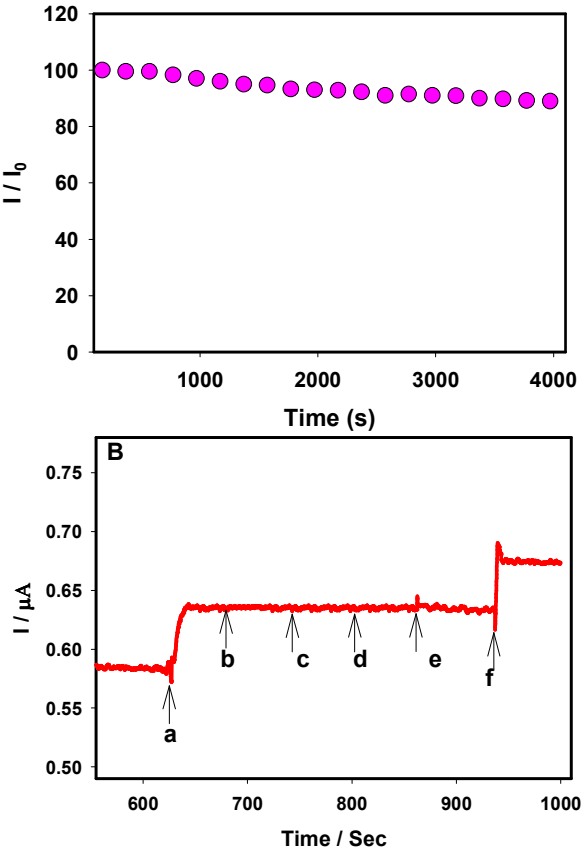

Fig. 6. (A) Stability test: relative amperometric current responses of the ADH-SWCNT-rGO/GCE in 0.1M tris buffer containing 20 µM ethanol + 10 mM NAD^+ (E_{app}: 0.5V). (B) Interference tests: injection of 20 µM ethanol (a), 1.0 mM each of ascorbic acid (b), glutathione (c), glucose (d), uric acid (e) and 20 µM ethanol (f) at E_{app} of 0.5 V in the presence of 10 mM NAD^+ in a 0.1 M tris buffer.

View Article Online
DOI: 10.1039/C7AN00594F

The ADH-SWCNT-rGO biosensor was further investigated for stability, interference with co-existing molecules, and real sample applications. The stability of the biosensor was tested through amperometric measurements in a 0.1M tris buffer (pH 8.2) containing 20 µM ethanol and 10 mM NAD^+ at a constant applied potential of 0.50 V over 4000 s. As seen in Fig. 6A, the relative current was decreased by ~8% throughout the experiment, showing that the fabricated biosensor possessed high stability toward the detection of ethanol. The selectivity of the biosensor with possible coexisting molecules such as ascorbic acid, glutathione, uric acid and glucose was investigated with 20 µM ethanol+ 10 mM NAD^+ in presence of 1.0 mM of each of these potential interfering molecules. As shown in Fig. 6B, there were no significant changes in the current response, prior to and following the addition of interfering molecules, which confirmed that the proposed ADH-SWCNT-rGO biosensor possessed a highly selective response to ethanol. We also further examined the proposed biosensor to demonstrate its capacity for practical applications. The determination of ethanol in serum, wine and beer using the standard addition method is presented in Table 1. High recoveries in the range of between 93% - 105% were achieved through the actual sample analysis, confirming that the developed biosensor is applicable for practical ethanol detection across a wide variety of samples.

Table 1: Determination of ethanol in real samples by the optimized ADH-SWCNT-rGO/GCE biosensor.

Sample	Concentration added (mM)	Concentration detected (mM)	Recovery (%)	RSD (%)
	10.00	9.30	93.0	3.3
Wine	20.00	19.80	98.9	2.4
	30.00	29.91	99.7	4.1
	10.00	9.82	98.2	1.9
Beer	20.00	20.06	100.3	3.6
	30.00	29.55	98.5	2.1
	10.00	10.40	104.0	4.3
Blood alcohol	20.00	20.30	102.0	4.7
	30.00	31.00	105.0	1.6

Conclusion

In this study, a novel biosensor platform has been designed based on the SWCNT–rGO nanohybrid with the assistance of the MADQUAT polymer for enzyme entrapment. The entrapped ADH was assessed for any conformational changes through secondary structure analysis, revealing that no structural change occurred in comparison to the free ADH. A significant synergisticenhancement of the SWCNT-rGO nanohybrid was confirmed, and the ADH entrapped by MADQUAT showed high activity for the detection of ethanol. The developed ADH-SWCNT-rGO biosensor exhibited high sensitivity with a remarkable low detection limit of 0.16 µM. The wide linear detection range, high stability and selectivity with a low K_m value make this biosensor a promising candidate for ethanol sensing in both clinical and environmental settings. The SWCNT-rGO nanohybrid and MADQUAT used in this study not only provide an excellent platform for the ethanol detection, but will also have significant impacts in the field of the development of high-performance enzymatic biosensors for food, clinical and environmental applications.

Acknowledgements

This work was supported by a Discovery Grant from the Natural Sciences and Engineering Research Council of Canada (NSERC RGPIN-2015-06248). B.R.A. thanks NSERC for the Postgraduate Scholarship. A.C. acknowledges NSERC and the Canada Foundation for Innovation (CFI) for the Canada Research Chair Award in Materials & Environmental Chemistry.

Notes and references

1 S. Zhang, Y. Xu, B. Wang, W. Qiao, D. Liu and Z. Li, *J. Control. Release,* 2004*,* **100**, 165-180.
2 É. Moreau, I. Ferrari, A.S. Drochon, P. Chapon, M. Vert and D. Domurado, *J. Control. Release,* 2000, **64,** 115-128.
3 E. Gorecka and J. Magdalena, *Biotechnol. Food Sci.,* 2011*,* **75**, 65-86.
4 N. Ormategui, A. Veloso, G.P. Leal, S. Rodriguez-Couto and R. Tomovska, *ACS Appl. Mater. Interfaces*, 2015*,* **7***,* 14104-14112.
5 C.A. Weatherly, R.M. Woods and D.W. Armstrong, J. Agric. Food Chem., 2014, **62**, 1832-1838.
6 X. Jia, S. Dong and E. Wang, *Biosens. Bioelectron.,* 2016, **76**, 80-90.
7 T. Cao, F. –T. Zhang, L. Y. Cai, Y. L. Zhou, N. J. Buurma and X.-X. Zhang, *Analyst*, *2017*, **142**, 987-993.
8 A.M. Azevedo, D.M. Prazeres, J.M. Cabral and L.S.P. Fonseca, *Biosens. Bioelectron.* 2005, **21**, 235-247.
9 H. Jornvall, J. Hedlund, T. Bergman, Y. Kallberg, E. Cederlund and B. Persson, *Chem. Biol. Interact.,* 2013, **202**, 91-96.
10 M. Zhang, W. Gorski, *Electroanal.,* 2011, **23**, 1856-1862.
11 M. Zhang, C. Mullens, W. Gorski, *Anal. Chem.,* 2007, **79**, 2446-2450.
12 H. Jornvall, *Eur. J. Biochem.,* 1977, **72**, 425-442.
13 J.L. Bennetzen and B.D. Hall, *J. Biol. Chem.,* 1982, **257**, 3018-3025.
14 C. Zhu, G. Yang, H. Li, D. Du, and Y. Lin, *Anal. Chem.,* 2014, **87**, 230-249.

View Article Online
DOI: 10.1039/C7AN00594F

15 M. Eguílaz, F. Gutierrez, J.M. González-Domínguez, M.T. Martínez and G. Rivas, *Biosens. Bioelectron.,* 2016, **86**, 308-314.
16 M. Govindhan, M. Amiri and A. Chen, *Biosens. Bioelectron.,* 2015, **66**, 474-480.
17 M. Zhang, A. Smith, W. Gorski, *Anal. Chem.*, 2004, **76**, 5045-5050.
18 M. Wooten, W. Gorski, *Anal. Chem.,* 2010, **82**, 1299–1304.
19 R. Zhang and X. Wang, *Chem. Mater.,* 2007, **19**, 976-978.
20 T. Yang, N. Zhou, Y. Zhang, W. Zhang, K. Jiao and G. Li, *Biosens. Bioelectron.,* 2009, **24**, 2165-2170.
21 B.R. Adhikari, M. Govindhan and A. Chen, *Sensors,* 2015, **15**, 22490-22508.
22 Chen and S. Chatterjee, *Chem. Soc. Rev.,* 2013, **42**, 5425-5438.
23 C. Gao , Z. Guo , J.-H. Liu and X.-J. Huang, *Nanoscale*, 2012, **4**, 1948-1963.
24 D. A. C. Brownson and C. E. Banks, *Analyst*, 2010, **135**, 2768–2778
25 D. A. C. Brownson, D. K. Kampouris and C. E. Banks, *Chem. Soc. Rev.*, 2012, **41**, 6944–6976
26 Z. Ayazi, *Analyst*, 2017, **142**, 721-739.
27 L. Kalantar-zadeh and J. Z. Ou, *ACS Sens.* 2016, **1**, 5-16.
28 F.-L. Meng, Z. Guo, X.-J. Huang, *Trends Anal. Chem.,* 2015, **68**, 37-47.
29 B.-R. Adhikari, M. Govindhan, H. Schraft and A. Chen, *J. Electroanal. Chem.,* 2016, **780**, 241-248.
30 X. Mao, F. Simeon, G.C. Rutledge and T. A. Hatton, *Adv. Mater.,* 2013, **25**, 1309-1314.
31 M. Baldassarre, A. Scire, I. Fiume and F. Tanfani, *Biochimie,* 2011, **93**, 542-548.
32 N .M. Huang, H. N. Lim, C. H. Chia, M. A. Yarmo and M. R. Muhamad, *Int. J. Nanomed.,* 2011, **6**, 3443-3448.
33 B. R. Adhikari, M. Govindhan and A. Chen, *Electrochim. Acta,* 2015, **162**, 198-204.
34 W. Putzbach and N. J. Ronkainen, *Sensors,* 2013, **13**, 4811-4840.
35 Y. Umasankar, R. P. Ramasamy, *ChemElectroChem*., 2014, **1**, 1834-1839.
36 R. Murphy, J. N. Coleman, M. Cadek, B. McCarthy, M. Bent, A. Drury, R. C. Barklie, and W. J. Blau, *J. Phy. Chem. B,* 2002, **106**, 3087-3091.
37 F. Secundo and G. Carrea, *Biotech. Bioeng.,* 2005, **92**, 438-446.
38 34 A. Natalello, A. M. I. Diletta, S. Brocca, M. Lotti, and S. M. Doglia, *Biochem. J.,* 2005, **385**, 511-517.
39 A. Tzialla, I. V. Pavlidis, M. P. Felicissimo, P. Rudolf, D. Gournis and H. Stamatis, *Bioresour. Technol,* 2010, **101**, 1587-1594.
40 S. B. Raj, S. Ramaswamy and B. P. Plapp, *Biochemistry,* 2014, **53**, 5791-5803.
41 S. Svensson, J. O. Höög, G. Schneider and T. Sandalova, *J. Mol. Biol.,* 2000, **302**, 441-453.
42 E. Abuin, E. Lissi and L. León, *Protein J.,* 2008, **27**, 247-252.
43 B. I. Cerda-Cristerna, S. Cottin, L. Flebus, A. Pozos- Guillén, H. U. Flores, E. Heinen, O. Jolois, C. Gérard, G. Maggipinto, and C. Sevrin, *Biomacromolecules,* 2012, **13**, 1172-1180.
44 L. Wu, X. Zhang and H. Ju, *Anal. Chem.,* 2007, **79**, 453-458.
45 P. Du, S. Liu, P. Wu, and C. Cai, *Electrochim. Acta,* 2007, **53**, 1811-1823.
46 E. Sharifi, E. Salimi and E. Shams, *Biosens. Bioelectrons.,* 2013, **15**, 260-266.
47 K. Guo, K. Qian, S. Zhang, J. Kong, C. Yu and B. Liu, *Talanta,* 2011, **85**, 1174-1179.
48 J. Manso, M. L. Mena, P. Yáñez-Sedeño and J. M. Pingarrón, *Electrochim. Acta,* 2008, **53**, 4007-4012.
49 C. Shan, H. Yang, D. Han, Q. Zhang, A. Ivaska and L. Niu, *Biosens. Bioelectron.,* 2010, **25**, 1504-1508.
50 R. A. Kamin and G. S. Wilson, *Anal. chem.,* 1980, **52**, 1198-1205.
51 B. Kowalewska and P. J. Kulesza, *Anal. Chem.,* 2012, **84**, 9564-9571.

View Article Online
DOI: 10.1039/C7AN00594F

Table of Contents Entry

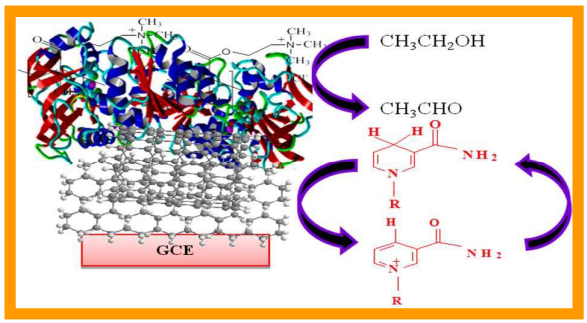

An efficient enzyme entrapment approach using cationic polymer has been demonstrated for the development of a high-performance ethanol biosensor.